Computers and Geotechnics 168 (2024) 106118

Contents lists available at ScienceDirect

Computers and Geotechnics

journal homepage: www.elsevier.com/locate/compgeo

Research paper

A continuum–discrete multiscale methodology using machine learning for thermal analysis of granular media

Rafael L. Rangel [a,b], Juan M. Gimenez [a,c,*], Eugenio Oñate [a,b], Alessandro Franci [a,b]

[a] Centre Internacional de Mètodes Numèrics a l'Enginyeria (CIMNE), 08034 Barcelona, Spain
[b] Universitat Politècnica de Catalunya (UPC BarcelonaTech), 08034 Barcelona, Spain
[c] Centro de Investigaciones de Métodos Computacionales (CIMEC), UNL/CONICET, 3000 Santa Fe, Argentina

ARTICLE INFO

Keywords:
Granular materials
Thermal behavior
Hierarchical multiscale
Continuum–discrete modeling
Machine-learning

ABSTRACT

This work presents a data-driven continuum–discrete multiscale methodology to simulate heat transfer through granular materials. The two scales are hierarchically coupled, where the effective thermal conductivity tensor required by the continuous method at the macroscale is obtained from offline microscale analyses. A set of granular media samples is created through the Discrete Element Method (DEM) to relate microstructure properties with thermal conductivity. The protocol for generating these Representative Volume Elements (RVEs) and homogenizing the microscale response is presented and validated by assessing the representativeness of the granular assemblies. The study found that two local properties, the porosity and the fabric of the material, are sufficient to accurately estimate a representative thermal conductivity tensor. The created dimensionless database of microscale results is used for training a surrogate model based on machine learning. In this way, effective thermal conductivity tensors that accurately reflect the local microstructure can be efficiently predicted from the surrogate model by taking the microstructural properties as inputs. The proposed multiscale methodology enables us to solve heat problems in granular media using a continuum approach with accuracy comparable to a pure discrete computational method but at significantly reduced computational cost.

1. Introduction

Granular media are ubiquitous in nature and are the most processed material in the industry after water. The thermal behavior of these materials is relevant in several situations, including static and dynamic systems. For example, in granular mixing with rotating drums (Rangel et al., 2023) or bladed stirrers (Kisuka et al., 2023), additive manufacturing by selective laser sintering (Kruth et al., 2003), packed and moving beds of catalytic reactors (Zhou et al., 2009), latent heat storage systems (Ismail and Henrıquez, 2002), landslides powered by heat-induced shear failures (Voight and Faust, 1992), among many other cases. It is therefore of paramount importance to develop effective and efficient numerical strategies for simulating heat transfer within granular media.

The particulate nature of granular materials gives them unique physical properties and makes the numerical modeling of their behavior a challenging task (Herrmann and Luding, 1998; Campbell, 2006). Typically, two different approaches are employed for the modeling of granular media: continuous and discrete methods. On the one hand, continuum-based methods are more computationally efficient but less accurate for representing microscale effects from grain interactions, which govern the overall behavior of the material. These methods resort to complex constitutive laws, most often phenomenological, which are mostly incapable of reproducing the grain-scale interactions or require several parameters of difficult calibration. On the other hand, discrete methods, which represent the granular medium as a collection of individual particles interacting with each other, enable a more accurate simulation of granular behavior. However, it comes with a much higher computational cost, mainly due to the substantial number of particles needed to represent real-world scenarios and the small time step required by these methods. Therefore, hybrid methodologies were developed to mitigate the limitations of continuum and discrete methods and harness their advantages by combining the two approaches either in a concurrent or in a hierarchical way (Andrade and Tu, 2009; Andrade et al., 2011; Yue et al., 2018; Cheng et al., 2023).

In hierarchical multiscale approaches (Borja and Wren, 1995; Guo and Zhao, 2014, 2016; Liang and Zhao, 2019; Guo et al., 2021; Liang et al., 2023), a continuous method is used to model the granular medium at the macroscale and the constitutive behavior arises from the homogenization of the discrete response at the microscale based

* Corresponding author at: Centre Internacional de Mètodes Numèrics a l'Enginyeria (CIMNE), 08034 Barcelona, Spain.
E-mail address: jmgimenez@cimne.upc.edu (J.M. Gimenez).

https://doi.org/10.1016/j.compgeo.2024.106118
Received 30 October 2023; Received in revised form 10 January 2024; Accepted 22 January 2024
Available online 8 February 2024

on Representative Volume Elements (RVEs). Several researches were carried out using this methodology, but only a few explored the thermal behavior of granular materials (Zhang et al., 2011; Zhao et al., 2020, 2022). Additionally, this multiscale strategy still lacks computational efficiency as the discrete response needs to be solved at several RVEs and, in the case of dynamic systems, at every time step of the macroscale solution. Therefore, data-driven computations of the discrete response have recently been employed to reduce the computational cost (Wang and Sun, 2018, 2019; Ma et al., 2022; Qu et al., 2023). A worthy strategy, developed in the context of turbulent flows, is introduced in Idelsohn et al. (2020) and Gimenez et al. (2021). The key feature of these multi-scale data-driven methods is that the most expensive stage of the computations, *i.e.*, the microscale solution, is performed offline. In particular, a sufficiently large number of RVE simulations is first performed to create a database of discrete responses, which is then used to train surrogate models, usually based on machine learning (ML) tools. Therefore, the online computations only involve the macroscale continuum solver, which receives the synthesized microscale discrete information directly from the surrogate model.

This work presents a methodology that combines the continuum–discrete hierarchical multiscale concept with a data-driven offline computation of the discrete response to simulate heat conduction across static granular media. The microscale computations over the RVEs are performed using the Discrete Element Method (DEM) (Cundall and Strack, 1979). An easy yet efficient protocol for RVE generation and homogenization is presented and analyzed. Special attention is devoted to demonstrating the so-called representativeness of the microscale response given by the granular assemblies. For this purpose, RVEs with different numbers of particles are examined in order to find the best balance between representativeness and computational cost of the microscale analysis. The identified setup of particles is then simulated under various conditions by altering its microstructural properties, such as porosity and fabric. The results of these DEM analyses on the RVEs are stored in a database that relates the thermal conductivity of the granular material with its microstructural properties. The thermal conductivity is expressed in a dimensionless form to allow the reuse of the database for other granular materials with different properties but the same particle size distribution and heat transfer model. This microscale database is then utilized for training an ML-based surrogate model for the conductivity–porosity–fabric relationship. Finally, the local effective thermal conductivity tensors of a granular medium, which are required for the continuous solution at the macroscale, are obtained from the ML-based surrogate model by taking the local microstructural properties as inputs and scaling the output tensors by the material's thermal conductivity.

This study demonstrates that the overall data-driven continuum–discrete multiscale method enables us to solve the heat problem in granular media with accuracy comparable to a pure discrete computational method but at significantly reduced computational cost. Furthermore, this study also provides interesting evidence of the effects of microstructure on macroscale responses. For instance, the presented numerical results show that thermal conductivity is intrinsically related to the local porosity and fabric of the material. Therefore, these properties alone are sufficient to estimate effective thermal conductivity tensors that accurately reflect the local microstructure. In fact, obtaining information about local porosity and fabric is necessary for the methodology to be put into practice. Fortunately, several non-destructive experimental and theoretical techniques exist for acquiring these microstructural properties of granular media in their natural state, including digital image analysis (Yang et al., 2008), X-ray computed tomography (Vlahinić et al., 2014; Wiebicke et al., 2020), and estimation from macroscopic material parameters, such as the elastic moduli (La Ragione and Magnanimo, 2012).

The generality of the proposed methodology and the clear separation between online macroscale computations and offline microscale ones permit a flexible computational structure and facilitate the implementation of the method. For instance, the macroscale analysis can be carried out using various numerical strategies for solving continuum mechanics problems. In this work, we employ the Finite Volume Method (FVM) (Versteeg and Malalasekera, 2007), but other numerical methods, such as the Finite Element Method (FEM) (Zienkiewicz et al., 2005), can also be used safely. Moreover, due to the decoupling between online and offline tasks, distinct computational platforms can be employed for micro and macroscale solutions and for training the surrogate model. In this work, we utilize two different open-source platforms for the two scales: Kratos Multiphysics (Dadvand et al., 2010) for the DEM microscale computations and OpenFOAM (Weller et al., 1998) for the FVM macroscale analysis.

The overall complexity of the multiscale analysis led us to some simplifying assumptions. Firstly, this study focuses solely on two-dimensional analysis. Considering the generality of the proposed approach, its extension to three-dimensional problems should not pose significant difficulties, except for the increased computational demand for database generation and online continuum computations. Furthermore, while we consider different particle sizes (polydisperse size distribution), we restrict our study to particles with the same shape (circular) and material properties. Lastly, we do not account for the effect of air within the RVE.

The remainder of this paper is structured as follows. Section 2 describes the proposed methodology by presenting the formulations of the continuous (FVM) and discrete (DEM) methods used at the macroscale and microscale, respectively. It also explains the protocol for generating and evaluating RVEs and the process of creating the database of microscale results and training the ML-based surrogate model. Section 3 presents the results of a convergence study on the number of particles used in the RVEs. It also shows the database of microscale results generated for a given granular material and the specific artificial neural network (ANN) trained. Additionally, the proposed methodology is validated by comparing the results of a microscale-informed continuous model with a pure DEM model. Finally, Section 4 provides some concluding remarks and suggestions for future developments.

2. Methodology

The macroscale solution of the heat transfer problem is achieved with a continuous numerical method by using, at each integration point, the effective thermal conductivity tensor derived from the local microstructure. Based on the knowledge of local porosity, η, and fabric tensor, $\boldsymbol{F}$, the effective thermal conductivity tensor, $\boldsymbol{K}$, is obtained from a database that relates these three parameters through a ML-based surrogate model. This database is created by generating several RVEs with the DEM. Each RVE is characterized by a different pair of porosity-fabric and the corresponding thermal conductivity tensor is computed by homogenization of the DEM solution. The thermal conductivity tensors are stored in a dimensionless form, $\widetilde{\boldsymbol{K}}$, in the database and must be scaled by the thermal conductivity of the material, k, before being assigned to the continuous model (*i.e.*, $\boldsymbol{K} = k\widetilde{\boldsymbol{K}}$). A general scheme of the methodology is presented in Fig. 1.

2.1. Macroscale formulation

At the macroscale, a transient heat diffusion problem is solved with a continuous numerical method. Therefore, the thermal behavior in a domain Ω of boundaries Γ is ruled by the volume-averaged heat diffusion equation and its boundary conditions, expressed as:

$$\begin{aligned} \rho c_p \frac{\partial T}{\partial t} &= \nabla \cdot (\boldsymbol{K} \nabla T) \quad \text{in} \quad \Omega \\ T &= \overline{T} \quad \text{in} \quad \Gamma_{\mathrm{D}} \\ \boldsymbol{K} \nabla T \cdot \boldsymbol{n}_{\Gamma} &= \overline{q} \quad \text{in} \quad \Gamma_{\mathrm{N}} \end{aligned} \tag{1}$$

where T is the unknown temperature field. The product ρc_p is the effective thermal inertia of the granular material, being ρ the density and c_p

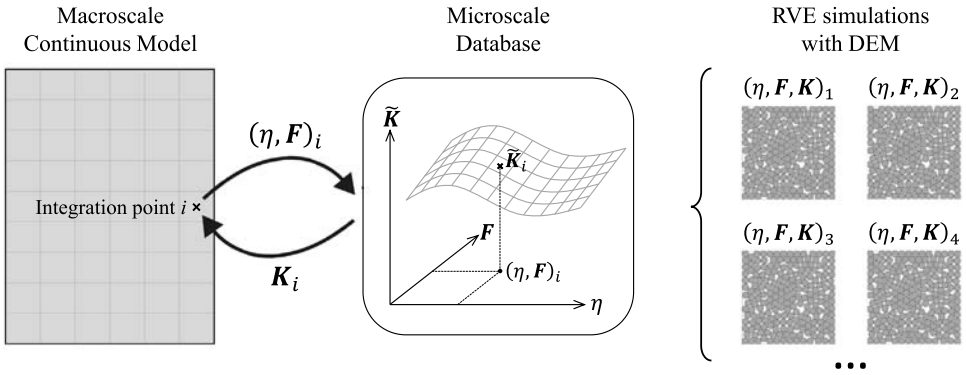

Fig. 1. General overview of the proposed continuum–discrete hierarchical multiscale method.

the heat capacity. By neglecting the thermal inertia of the air, we can assume that $\rho c_p = \rho_s c_{p,s}(1-\eta)$, where the subscript s indicates properties of the solid grains and η is the porosity, which is defined as the ratio of the void volume to the averaging volume. The effective thermal conductivity tensor, $\boldsymbol{K}$, depends on microstructural properties of the granular medium, which will be computed from microscale discrete analyses. On Dirichlet boundaries, Γ_{D}, $\overline{T}$ is the imposed temperature, while on Neumann boundaries, Γ_{N}, $\overline{q}$ is the applied heat flux. The unit vector $\boldsymbol{n}_\Gamma$ denotes the outwards normal to the boundary.

The solution of the transient diffusion problem of Eq. (1) can be obtained using standard numerical methods. In this work, the spatial discretization and the solution of the partial differential equation are done via the cell-centered Finite Volume Method (FVM). For this purpose, the domain Ω is split into non-overlapped volumes Ω_j such that $\Omega = \bigcup_j \Omega_j$ and $0 = \bigcap_j \Omega_j$. A cell Ω_j is an arbitrary polyhedron whose boundary Γ_j is composed by flat faces b of normal $\boldsymbol{n}_b$ and area Γ_b, such that $\Gamma_j = \bigcup_b \Gamma_b$. The unknown field, T_j, and the other material properties are stored in the cell center and linearly interpolated to the face mid-points when required. Therefore, after discretization and local balance procedures, the algebraic equation system is expressed as:

$$\sum_j \left((\rho c_p)_j \left(\frac{\partial T}{\partial t} \right)_j \Omega_j - \sum_{b \in \Gamma_j} (\boldsymbol{K} \cdot \nabla T \cdot \mathbf{n})_b \, \Gamma_b \right) = 0. \tag{2}$$

For the computational implementation, we used the open-source library OpenFOAM as the basis. Within this framework, we developed our own solver to tackle the transient diffusion problem considering a spatially variable diffusion tensor. We employ an implicit first-order operator for the temporal term and second-order operators for the spatial approximations.

2.2. Microscale formulation

At the microscale, the DEM is applied to simulate the granular behavior. For the mechanical behavior, the translational and rotational motions of each particle are solved by explicitly integrating the following equilibrium equations:

$$m \frac{\mathrm{d}\boldsymbol{v}}{\mathrm{d}t} = \boldsymbol{f} \tag{3}$$

$$I \frac{\mathrm{d}\omega}{\mathrm{d}t} = M \tag{4}$$

where m, I, $\boldsymbol{v}$, ω, $\boldsymbol{f}$ and M are the mass, moment of inertia, translational velocity, angular velocity, resulting force and resulting torque of a particle, respectively.

The resulting force acting on a particle is given here by the sum of the contact forces with each neighbor and a non-viscous damping force. In this work, simple linear models of contact forces are adopted. The normal contact force between a particle and a neighbor, $\boldsymbol{f}_{cn}$, is calculated as:

$$\boldsymbol{f}_{cn} = -s_n \delta_n \boldsymbol{n} \tag{5}$$

where s_n is the normal contact stiffness, δ_n is the contact overlap, and $\boldsymbol{n}$ is the unit outward normal of the contact.

The tangential contact force, $\boldsymbol{f}_{ct}$, is calculated incrementally and subjected to Coulomb's friction condition, as:

$$\boldsymbol{f}_{ct} = \begin{cases} \boldsymbol{f}_{ct}^{\mathrm{prev}} - s_t \Delta \boldsymbol{u}_t & \text{if } |\boldsymbol{f}_{ct}| \le |\boldsymbol{f}_{cn}| \tan(\varphi) \\ |\boldsymbol{f}_{cn}| \tan(\varphi)\, \boldsymbol{t} & \text{otherwise} \end{cases} \tag{6}$$

where $\boldsymbol{f}_{ct}^{\mathrm{prev}}$ is the tangential force of the previous time step, s_t is the tangential contact stiffness, $\Delta \boldsymbol{u}_t$ is the increment of relative tangential displacement at the contact, $\boldsymbol{t}$ is the unit vector along the tangential direction of the contact, and φ is the contact friction angle.

The normal and tangential stiffnesses are calculated as follows:

$$s_n = 2e \frac{r_1 r_2}{r_1 + r_2} \tag{7}$$

$$s_t = \nu s_n \tag{8}$$

where e and ν are, respectively, Young's modulus and tangential-to-normal stiffness ratio of the contacting elements, and r_1 and r_2 are their radii. If the neighbor is a wall element, only the radius of the particle is considered (*i.e.*, $s_n = 2er_1$).

The damping force, $\boldsymbol{f}_d$, is added to each particle in the opposite direction of its velocity to dissipate kinetic energy. It is calculated with the damping coefficient, μ, and the resulting contact force of the particle with all its neighbors, $\boldsymbol{f}_c$, as:

$$\boldsymbol{f}_d = -\mu |\boldsymbol{f}_c| \frac{\boldsymbol{v}}{|\boldsymbol{v}|} \tag{9}$$

Finally, the resulting torque acting on a particle is given by the sum of the torques caused by each neighbor, which are simply calculated as the product of the tangential force by its lever arm with respect to the particle's longitudinal axis. Rolling resistance is not taken into account.

For the thermal behavior, particles are considered isothermal and the temperature of each is calculated by explicitly integrating the following equation:

$$m c_p \frac{\mathrm{d}T}{\mathrm{d}t} = q \tag{10}$$

where q is the net heat transfer to the particle from all its neighbors in the current time step.

In this work, it is assumed that heat flux happens only by thermal conduction through the contact area. The heat transferred to a particle from one of its neighbors, q_c, is calculated with a thermal pipe model as follows:

$$q_c = -k a_p \frac{\Delta T}{l_p} \tag{11}$$

where k is the thermal conductivity of both elements in contact, ΔT is the temperature difference between the particle and its neighbor, and a_p and l_p are, respectively, the cross-sectional area and the length of the thermal pipe.

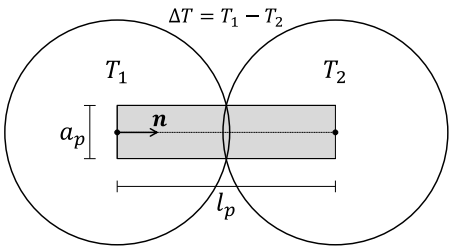

Fig. 2. In-plane illustration of the thermal pipe model used to calculate the heat flux between particles (the thermal pipe is shaded).

In this work, for simplicity, we focus on two-dimensional (2D) problems only. Consequently, we represent the grains with cylindrical particles (rods) of unit length, all moving within the same plane. As a result, the cross-sectional area of the pipe is equivalent to the in-plane contact width, and the length of the pipe represents the distance between the particles' longitudinal axes. This is illustrated in Fig. 2. If the neighboring element is a wall, the pipe length is determined as the perpendicular distance between the particle's longitudinal axis and the wall.

2.3. RVE generation and evaluation

To obtain information from the microscale, we use Representative Volume Elements (RVEs). In this context, an RVE is a DEM assembly with a sufficient number of particles to statistically capture the material's constitutive behavior with good accuracy while maintaining the computational efficiency. In this section, we first describe the protocol of RVE generation and then explain the homogenization procedure used to upscale the microscale information.

As illustrated in the left picture of Fig. 3, the first step of our protocol for generating RVEs consists of randomly positioning a pre-established number of particles within a control domain. Subsequently, the particles are compacted by moving the boundaries of the domain inwards, without considering the effects of gravity, similar to what is done in other studies (Radjai and Dubois, 2011; Shahin et al., 2016). The initial size of the domain should be sufficiently large to grant significant freedom of movement to the particles during compression. Unlike the aforementioned works, in our protocol, the boundaries are made of frictionless flat wall elements. As it will be explained later, this feature has implications for the homogenization procedure. The wall elements are assigned the same material parameters as the particles, except for the friction angle, which is set to zero between particles and walls. During consolidation, the walls move at a constant speed equivalent to the mean particle radius per second, a relatively slow velocity in order to prevent excessive dynamic effects. To modify the final fabric of the RVE, the velocities can be adjusted independently among walls. The motion of the walls ends when the particle assembly reaches a pre-defined limit for a certain variable, which, in this work, is a threshold value of the porosity. Analogously to other protocols proposed in the literature, *e.g.*, in Berzi and Vescovi (2021), after stopping the motion of the walls, the simulation continues until the mechanical equilibrium of the system is reached. After this relaxation phase, the final positions of the particles and walls are used to compute the fabric and homogenize the thermal conductivity, as explained next.

The fabric of a granular material is commonly used to characterize its microstructure. Following the popular contact-based tensorial definition of Oda (1982), the fabric is computed as:

$$\boldsymbol{F} = \frac{1}{n_c}\sum_{c=1}^{n_c}(\boldsymbol{n}\otimes\boldsymbol{n})_c \tag{12}$$

where n_c is the total number of contacts in the RVE and $\otimes$ denotes the outer product.

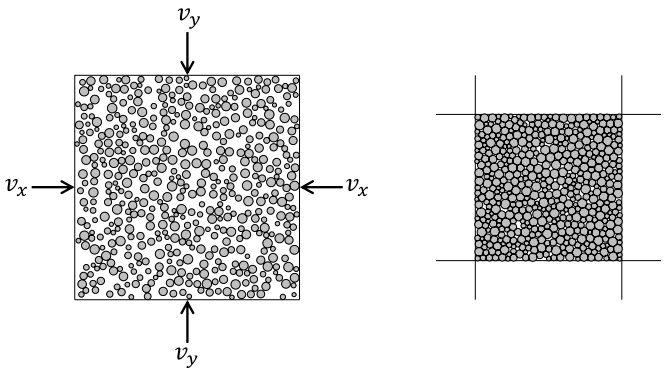

Fig. 3. RVE generation process: initial configuration with 500 particles (left) and final configuration with a target porosity after an isotropic compression (right).

The thermal conductivity of a discrete medium is homogenized into an effective thermal conductivity tensor, which is generically computed as:

$$\boldsymbol{K} = \frac{1}{V_{RVE}}\sum_{c=1}^{n_c}(\boldsymbol{K}al)_c \tag{13}$$

Analyzing Eq. (13), the thermal conductivity tensor of each contact is multiplied by a representative cross-sectional area, a, and length, l, over which the heat flows. The sum of this product over all contacts is divided by the homogenization volume, V_{RVE}, which is the volume of the RVE.

Using Fourier's law, the thermal conductivity tensor of the contact is expressed in terms of the heat flux vector, $\boldsymbol{q}$, and the temperature gradient in the normal direction of the contact, $(\nabla T\cdot\boldsymbol{n})\boldsymbol{n}$. Therefore, the effective thermal conductivity tensor can be expressed as:

$$\boldsymbol{K} = \frac{1}{V_{RVE}}\sum_{c=1}^{n_c}\left(-\boldsymbol{q}\otimes[(\nabla T\cdot\boldsymbol{n})\boldsymbol{n}]^{-1}\,al\right)_c \tag{14}$$

For the thermal pipe model of heat conduction presented in Eq. (11), the representative cross-sectional area is the cross-sectional area of the pipe ($a = a_p$) and the representative length is the length of the pipe ($l = l_p$). Moreover, according to this model, the heat flux vector and the temperature gradient are defined as follows:

$$\boldsymbol{q} = -k\frac{\Delta T}{l_p}\boldsymbol{n} \tag{15}$$

$$(\nabla T\cdot\boldsymbol{n})\boldsymbol{n} \approx \Delta T\left(l_p\boldsymbol{n}\right)^{-1} \tag{16}$$

Substituting Eqs. (15) and (16) into Eq. (14), one obtains the homogenized expression of the effective thermal conductivity tensor for the thermal pipe conduction model, which is:

$$\boldsymbol{K} = \frac{1}{V_{RVE}}\sum_{c=1}^{n_c}\left(ka_pl_p\boldsymbol{n}\otimes\boldsymbol{n}\right)_c \tag{17}$$

This expression relies only on geometric information of the problem, in addition to the thermal conductivity of the elements. Therefore, no heat is imposed on the RVEs as their thermal solution is not required to compute the homogenized conductivity tensor.

To mitigate local effects that may arise near the boundaries and thus improve the representativeness of the assembly, contact interactions with the walls and between particles touching a wall (peripheral particles) are not taken into account when evaluating the microstructural properties of the RVE. This means that only contacts involving a particle that is not touching a wall (internal particle) are considered for solving Eqs. (12) and (17). Consequently, due to the discarding of some contacts, the homogenization volume V_{RVE} must be reduced accordingly. Therefore, a convex hull delimiting the chain of the considered contacts is created to define the effective RVE volume (area with unit

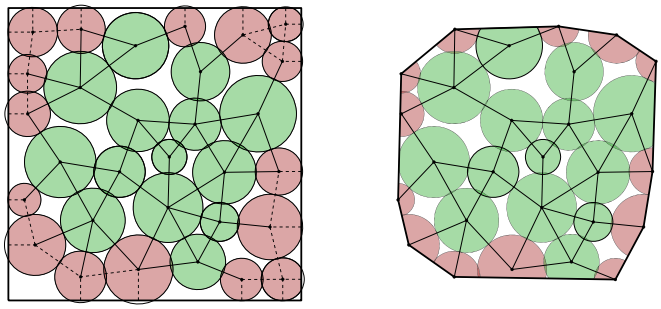

Fig. 4. Strategy to mitigate local effects near the walls illustrated for a small assembly of particles. Left: RVE showing internal particles (green fill), peripheral particles (red fill), considered contacts (continuous lines), and discarded contacts (dashed lines). Right: Convex hull delimiting the chain of considered contacts.

length in 2D), which is used to homogenize the thermal conductivity and to compute the porosity during the RVE compression phase. This strategy is illustrated in Fig. 4 for a small assembly of particles.

All computational implementations related to the microscale, including the generation of RVEs and the homogenization and evaluation of microstructural properties, were done in the open-source framework Kratos Multiphysics (Dadvand et al., 2010).

2.4. Microscale database and machine learning model

To create the database of microscale results, several RVEs need to be generated, each one with a different porosity and fabric, which are the inputs of the database. The target porosity is achieved by stopping the compression of the RVE when that value is reached, while the fabric is varied by changing the relative velocities of the walls. Therefore, by altering only the wall velocities while maintaining the same initial particle distribution, we are able to obtain different RVE configurations characterized by distinct pairs of porosity and fabric. Consequently, these configurations yield different effective thermal conductivity tensors after the homogenization procedure described in the previous section. The components of these tensors are divided by the thermal conductivity of the particles ($\widetilde{\boldsymbol{K}} = \boldsymbol{K}/k$) to make the database dimensionless and, thus, valid for any granular material that shares the same particle size distribution and is ruled with the same heat transfer model. The porosity, fabric tensor, and dimensionless thermal conductivity tensor of each of the created configurations are data points that are then stored in the microscale database. Due to the absence of gravity, the solution of square RVEs is frame invariant and, therefore, it is possible to multiply the number of data points by considering orthogonal rotation of axes. For instance, in 2D, we can duplicate the dataset by generating additional data points through a 90° rotation of the obtained thermal conductivity and fabric tensors with a rotation transformation matrix.

The dimensionless thermal conductivity tensors are the output of interest and the results stored in the microscale database can be considered as sample points of a continuous n-dimensional function Ψ, where n is the number of inputs of the database (in this case, two), *i.e.*:

$$\widetilde{\boldsymbol{K}} = \Psi(X), \qquad \text{with } X = (\eta, \boldsymbol{F}) \tag{18}$$

Therefore, it is necessary to define the multi-valuated and multi-dimensional function Ψ to predict the thermal conductivity for non-simulated points. For this objective, we employ artificial neural networks (ANN). An ANN is a massively parallel distributed processor made up of simple processing units that has a natural propensity for storing data-based knowledge and making it available for use (Haykin, 2009). ANNs are often used as a surrogate model or as a response surface approximation model because of their robustness in solving multivariate and nonlinear modeling problems, such as function approximations, optimization, and classification (Bre et al., 2018). Some authors have successfully used ANNs to predict or interpolate simulated data in multiscale approaches (Idelsohn et al., 2020; Gimenez et al., 2021).

In this work, a feed-forward multilayer network is used. The general ANN architecture has an input layer, a set of hidden layers, and an output layer. In each hidden and output layer, there are artificial neurons interconnected via adaptive weights. These weights are calibrated through a training process with input–output data. For each artificial neuron, the tangent sigmoid is selected as the activation function, except for the output layer, where linear functions are employed. The ANN training process is made with the Root Mean Square Propagation algorithm, considering the mean squared error (MSE) as the convergence indicator.

The coefficient of determination R-squared (R^2):

$$R^2 = 1 - \frac{\sum_{i=1}^{N}(D_i - P_i)^2}{\sum_{i=1}^{N}(D_i - [D])^2}, \tag{19}$$

is used to quantify the agreement, where D_i and P_i are the computed (via DEM) and predicted (via ANN) values for the sample i, respectively. The square brackets denote the mean value. A perfect agreement is obtained when R^2 is equal to one.

The validity of the surrogate model is guaranteed only within the range of values covered by the training data points, as extrapolated results are not reliable. Therefore, the microscale database and its ML-based surrogate model are valid for the range of porosity and fabric covered during the generation of RVEs.

3. Results and discussion

A granular material with the following properties is used for the investigations presented in this section: density of 2650 kg/m^3, Young's modulus of 600 MPa, tangential-to-normal stiffness ratio of 0.8, friction angle of 0.5, thermal conductivity of 100 W/mK, and heat capacity of 100 J/kgK. These values are fictitious material parameters solely intended for validating the proposed methodology. In addition, a damping coefficient of 0.1 is employed. The particle size distribution follows the one used in Guo and Zhao (2014) and is characterized by a constant function of the radius with mean, minimum and maximum values of 5.0 mm, 3.0 mm and 7.0 mm, respectively.

3.1. Representativeness of the RVEs

It is of crucial importance to determine an optimal number of particles in the RVEs that balances the representativeness of the microscale with the computational cost of its simulation. To calibrate the particles number for the described RVE generation and homogenization protocol, a convergence study was conducted by creating RVEs with seven different numbers of particles: 100, 200, 300, 500, 750, 1000, and 1500. For each number of particles, ten RVEs with distinct initial particle positions were generated in order to enhance the reliability of results and examine their variability. All RVEs were generated for the same porosity of 13% by isotropic compression (*i.e.*, orthogonal motion of walls with the same speed in horizontal and vertical directions). Two parameters are analyzed here to evaluate the convergence of results: the polar histogram of the particle contact network (rose diagram) and the homogenized thermal conductivity.

The rose diagram provides the distribution of contact normal directions. For an isotropic compression of the RVE, this distribution is expected to be approximately uniform, which corresponds to an isotropic fabric with no principal directions. Therefore, the uniformity of the diagrams has been qualitatively appraised, similarly to what is done in other works (Guo and Zhao, 2014; Meier et al., 2008). The resulting rose diagrams from one of the simulations of five different setups (100, 300, 500, 1000, and 1500 particles) are given in Fig. 5.

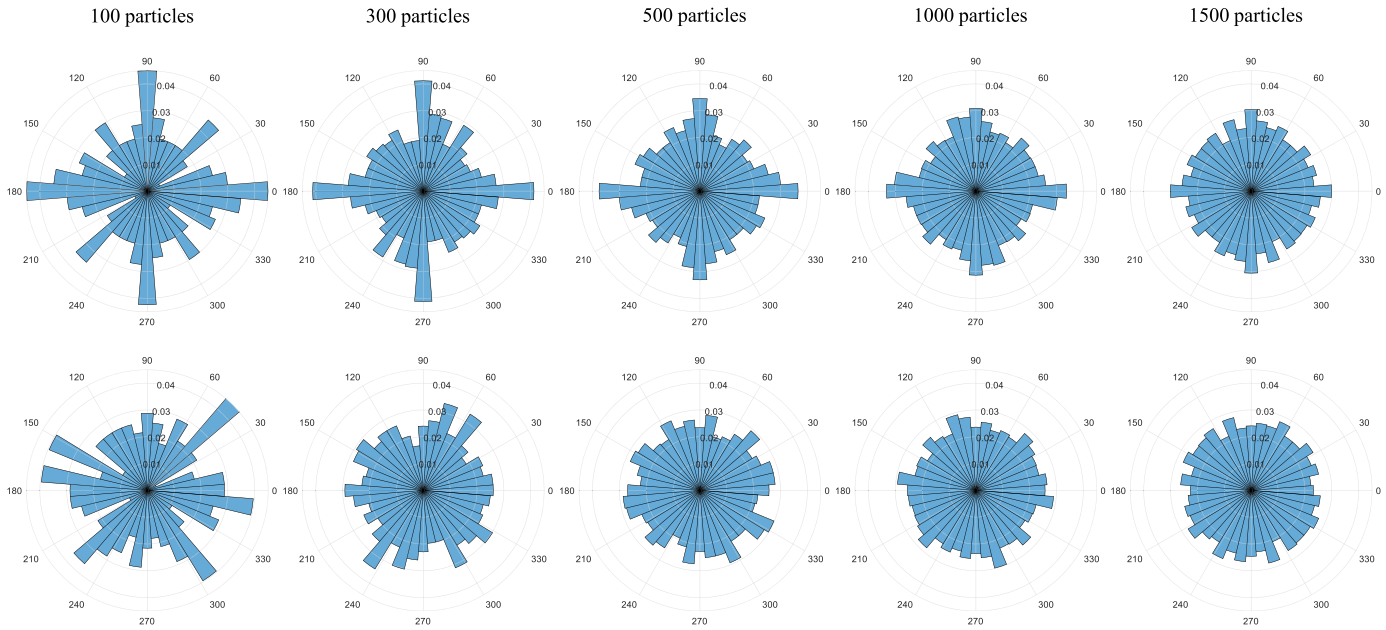

Fig. 5. Rose diagrams of RVEs with 100 to 1500 particles considering all contacts in the assembly (top row) and only contacts involving internal particles (bottom row).

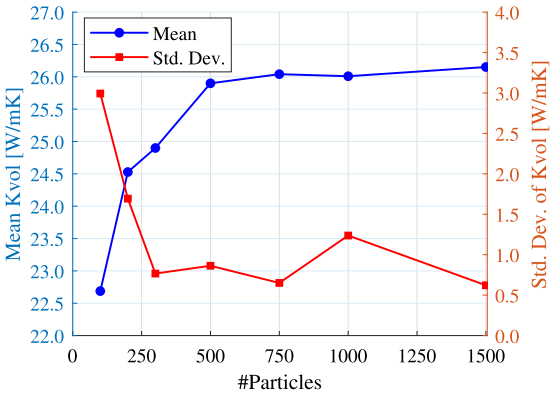

Fig. 6. Mean value and standard deviation of the volumetric component of the effective thermal conductivity tensor from RVEs with 100 to 1500 particles.

The top row shows the results considering all contacts in the assembly while the bottom row depicts the diagrams of the same RVEs obtained by considering only contacts involving internal particles, as proposed in Section 2.3. The diagrams are normalized with respect to the total number of contacts of each assembly.

From the rose diagrams in the top row of Fig. 5, the influence of the flat walls is clearly evident by the predominance of the horizontal and vertical contact directions. As the number of particles in the RVE increases, the effects of walls seem to reduce as the prominence of principal directions gradually diminishes. However, a very large amount of particles is needed to cease these effects. In fact, with 1500 particles the diagram presents a nearly uniform distribution of contacts (circular shape of the rose), but the horizontal and vertical directions still have a slight dominance. On the other hand, when applying the proposed procedure, as seen in the bottom row of Fig. 5, the wall effects on the fabric vanish as the horizontal and vertical directions no longer hold the majority of contacts. In addition, the diagrams seem to have converged to a nearly uniform distribution with only 500 particles, which suggests that this number of particles is sufficient to achieve a faithful representation of the microscale.

The homogenized thermal conductivity of granular assemblies with the same porosity and similar fabrics is expected to be approximately equal. Fig. 6 provides the mean value and the standard deviation of the volumetric component of the effective thermal conductivity tensor (*i.e.*, the average of the xx and yy components) obtained from the ten RVE simulations with each number of particles. The graph confirms that with 500 particles both metrics have approached a converged value. The simulations with this setup presented a standard deviation of 0.863 W/mK, which corresponds to a relative error of 3.3% with respect to the mean value, a precision considered sufficiently accurate. Therefore, 500 particles are chosen since they offer the best balance between representativeness and computational cost of the microscale analysis. We highlight that the average number of internal particles in the chosen RVEs, which are those effectively considered for the contact interactions, is 422. Notably, despite the differences in the RVE generation protocols, this number aligns with the range suggested in the literature for 2D RVEs, which typically spans between 200 (Kaneko et al., 2003) and 700 (Meier et al., 2008) particles. We also note that several similar studies recommend a value of 400 particles (Guo and Zhao, 2014; Shahin et al., 2016; Nitka et al., 2011; Nguyen et al., 2014).

3.2. Microscale surrogate model

A database of microscale results and an ML-based surrogate model are created for the given granular material. In order to reduce the number of input variables of the database, the fabric tensor is represented by a single scalar parameter. As defined in Eq. (12), the fabric tensor always has a trace of 1.0. Therefore, in a two-dimensional analysis, the diagonal components, F_{xx} and F_{yy}, can be synthesized into a single value, f, given by the difference $f = F_{xx} - F_{yy}$. In addition, since we only impose orthogonal motion to the boundaries of RVEs during compression (bi-axial consolidation), the resulting off-diagonal components of the fabric tensor, F_{xy} and F_{yx}, are always negligible. Therefore, we are able to take f as the sole parameter to represent the fabric of the RVE.

3.2.1. Database generation

The database of microscale results was created by generating RVEs with fixed porosity values ranging from 10.0% to 18.0% with increments of 0.5%. It is of great importance that the database encompasses a broad fabric spectrum to allow its applicability for diverse compaction conditions of the granular material. Therefore, for each porosity, multiple RVEs were generated by imposing different relative wall speeds

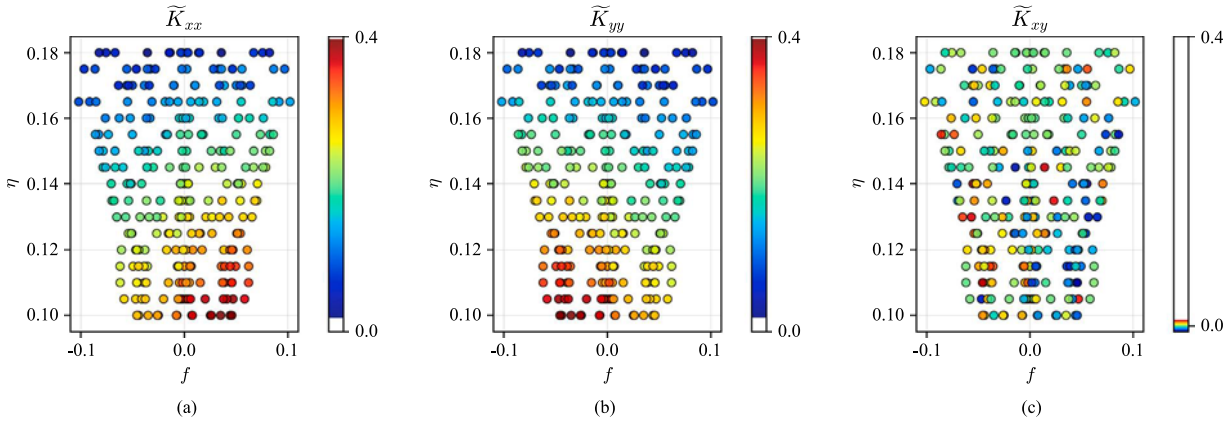

Fig. 7. Database of microscale results. Each pair (η, f) represents a generated data point where the components of the dimensionless thermal conductivity tensor $\widetilde{\boldsymbol{K}}$ are the output. The scatter diagrams (a), (b), and (c) depict the xx, yy, and xy components, respectively.

in the horizontal and vertical directions in order to widen the range of fabric values covered by the database. In particular, relative wall speeds ranging from an isotropic compression (same horizontal and vertical speeds) to a purely horizontal compression (only vertical walls move) were used.

In total, RVEs with 136 different configurations (porosity-fabric pairs and their corresponding thermal conductivity tensors) were generated, each one with a distinct initial particle distribution. Based on the assumption of invariance under orthogonal rotations, the solution of each RVE was rotated by 90° (*i.e.*, swapping the values of K_{xx} and K_{yy} and inverting the signs of K_{xy} and f) to give rise to a new data point, thus totaling 272 data points. The thermal conductivity tensors are made dimensionless by dividing their components by the thermal conductivity of the particles. The results are given in Fig. 7, where the data points are displayed on a color scale that represents the dimensionless value of each component of the thermal conductivity tensor. These results are available as supplementary material of this paper.

It can be observed that, due to the rotation of RVE solutions, the distribution of data points in the $f \times \eta$ plane is symmetric with respect to $f = 0$. For the same reason, the xx and yy components of the thermal conductivity tensors are mirrored with respect to each other. It is also noticeable that the range of fabric values tends to increase with porosity, even though RVEs were generated with the same compression conditions at every porosity level. Moreover, it is noteworthy that the value of f is complex to control precisely. However, in general, we observe that RVEs generated with a greater disparity between horizontal and vertical compression speeds tend to yield higher fabric values, while nearly zero fabric values are typically obtained from RVEs generated through isotropic compression.

Regarding the thermal conductivity, as expected, it is evident that the xx and yy components decrease with porosity and increase as the fabric components in their respective directions become more pronounced. In addition, because of the absence of shear motion in the RVEs, the values of the xy components are relatively very small and can be considered as spurious noises, similarly to the off-diagonal components of the fabric tensor. Therefore, these components are also assumed negligible henceforth.

3.2.2. Machine learning

The Artificial Neural Network (ANN) architecture selected for training the database of RVE results is presented in Fig. 8a. It has two input neurons (porosity and fabric) and two output neurons (the diagonal components of the dimensionless thermal conductivity tensor). There is not a general rule to define a proper ANN structure in terms of the number of hidden layers and artificial neurons, so, for this database, the ANN is formed by one hidden layer with 16 neurons and it was calibrated by trial and error. The ANN training was accomplished with a maximum of 5000 epochs. The dataset was randomly split into training and validation subsets, considering proportions of 80% and 20%, respectively. The learning curves are presented in Fig. 8b. The good fit is identified by training and validation loss curves decreasing to a point of stability with a minimal gap between the two final loss values. The loss of the model on the training dataset is slightly lower than the validation dataset; this small generalization gap guarantees no over-fitting, so the model can make accurate predictions on new, unseen examples.

The fitting of the xx and yy components of the dimensionless thermal conductivity tensors are presented through the scatter plots in Fig. 8c and Fig. 8d, respectively. These plots compare the DEM-computed and ANN-predicted conductivities for each input of the set, where the dashed line represents the ideal fitting of $R^2 = 1$. The obtained coefficients of determination ($R^2 = 0.972$ for K_{xx} and $R^2 = 0.971$ for K_{yy}) are considered sufficiently accurate. This is because these results mean that more than 97% of the variations of the thermal conductivity can be explained by the selected input parameters. Therefore, the good agreement between ANN and DEM is a strong indication that the input selection was correct. It corroborates that, based exclusively on the porosity and fabric, we can predict effective thermal conductivity tensors that reflect the local microstructure of a granular material with approximately 97% of accuracy. The fitting error of around 3% also aligns with the results presented in Section 3.1, specifically in Fig. 6, where a relative error of 3.3% was observed for the variation of the thermal conductivity of several 500-particle RVEs with the same porosity and similar fabrics. These unexplained fluctuations of the thermal conductivity are related to the influence of other potential parameters that are not being considered as inputs of the surrogate model because their impacts on the results are expected to be very small. It should be noted that the model's accuracy was achieved under certain conditions in this work: static regime, two-dimensional analysis, normal compression with no shear effects, and a single particle size distribution. In other scenarios, where these conditions are not met, different parameters may have a significant contribution and, therefore, they would need to be identified and included into the ANN-based surrogate model.

The ANN prediction surface for the xx component of the dimensionless thermal conductivity tensor is shown in Fig. 9a. The data points are also depicted, however, it should be noted that the conductivity values at these points are not necessarily the values given by the prediction surface. The bounding box of data points in the $f \times \eta$ plane (colored region) defines the validity region of the prediction surface, where the ANN fit is guaranteed and the interpolation of data is reliable. The gray region, on the other hand, requires extrapolation of data, which is not reliable from the employed algorithm. The variation of the

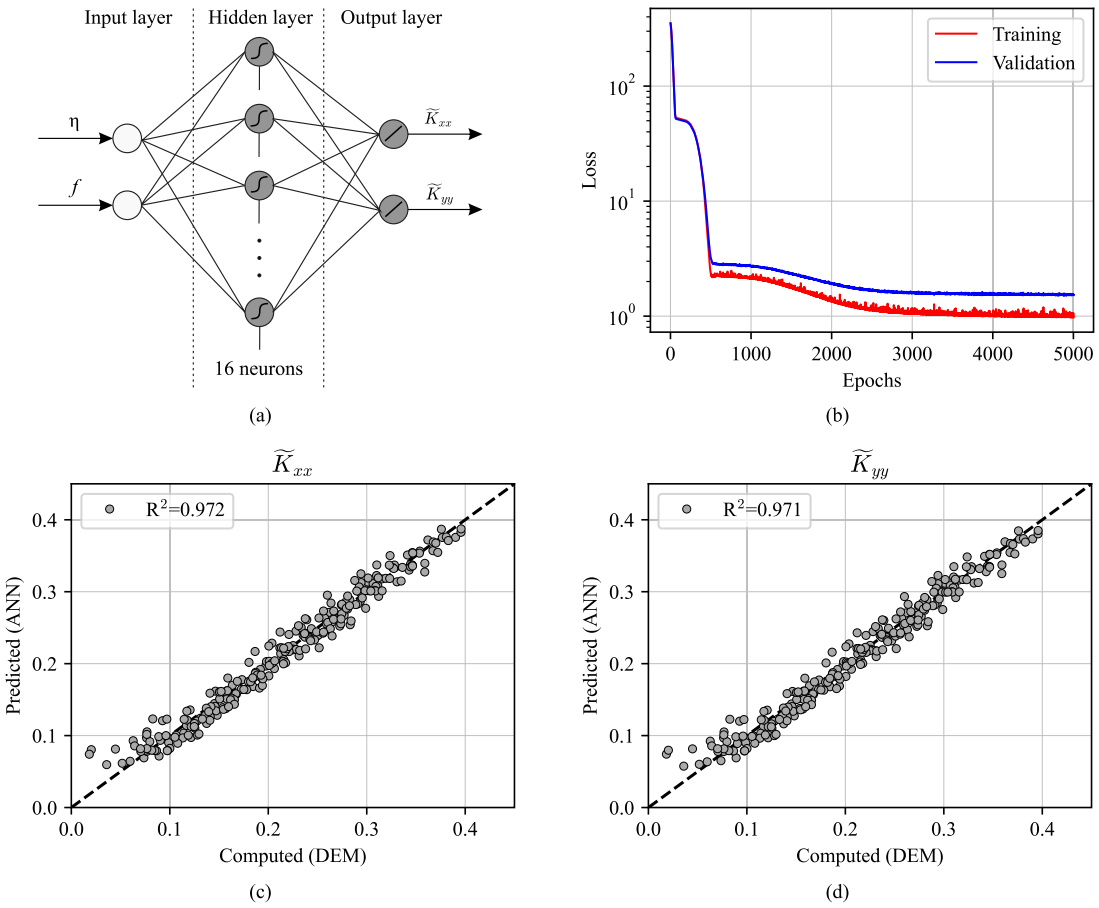

Fig. 8. (a) ANN architecture selected. (b) learning curves. (c-d) fitting of the ANN predictions against DEM outputs for the xx and yy components of the dimensionless thermal conductivity tensor, respectively.

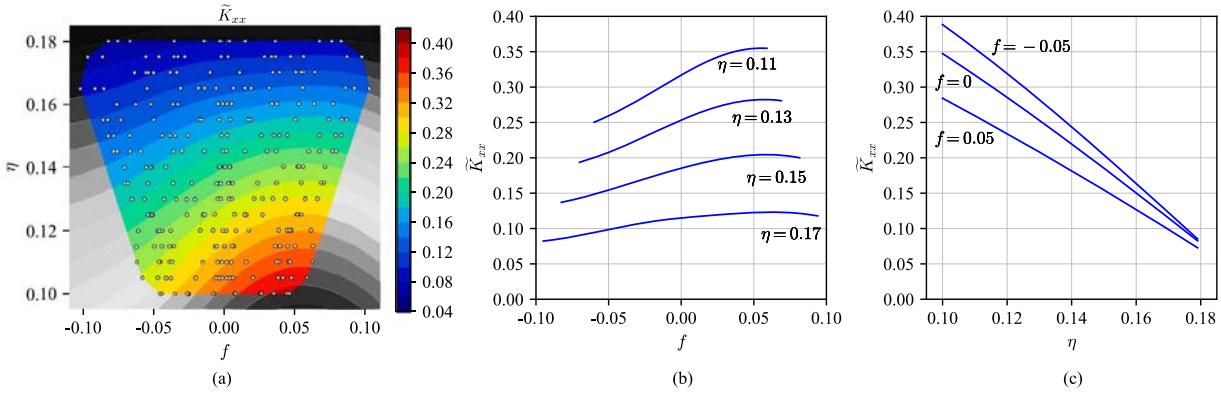

Fig. 9. (a) ANN prediction surface for the xx component of the dimensionless thermal conductivity tensors, where the colored region denotes the reliable (interpolation) region. Isolines of the ANN prediction surface for K_{xx} are shown for fixed values of (b) porosity and (c) fabric.

thermal conductivity for fixed values of the inputs is shown through the isolines of the prediction surface in Fig. 9b and Fig. 9c. Notably, the conductivity varies with a non-intuitive behavior with the fabric and almost linearly with the porosity.

We remark that a machine-learning tool is employed here for the sake of generality, as the ANN has only two inputs and, therefore, its outputs could be interpolated with a simpler strategy (*e.g.*, linear interpolation based on a Delaunay triangulation in the $f \times \eta$ plane). However, since the employed ANN has only one hidden layer, using such a high-dimensional mapping tool for the present case has negligible risk of over-fitting due to low dimensionality. This is evident in Fig. 9a, where the result is a smooth paraboloid-like surface. Moreover, the use of an ANN allows the methodology to be readily expanded to a function with more inputs, which would be the case when performing 3D simulations, accounting for shear effects in the RVEs, generalizing the database to different particle size distributions, or including mechanical behavior. In fact, as the number of input/output parameters increases, it is expected that deeper neural networks will be required.

3.3. Validation case

To validate the proposed methodology, the heat flux across a granular material is simulated with both discrete and continuous methods.

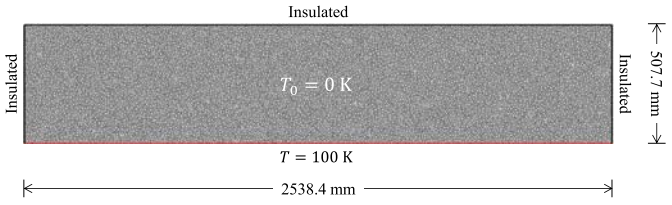

Fig. 10. Reference DEM model.

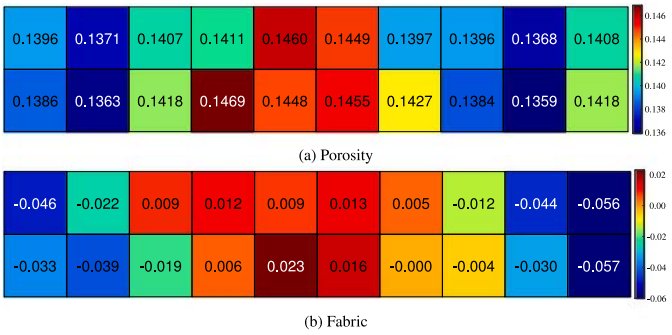

Fig. 11. Local properties of reference DEM model.

The DEM model is used as a reference solution, from which we are able to obtain local microstructural properties required for the continuum-based analysis. The FVM model is then solved in a multiscale fashion with microscale-informed local porosities and thermal conductivity tensors, so its solution is compared against the reference discrete model.

3.3.1. Reference DEM model

The reference DEM model is shown in Fig. 10 and consists of a rectangular box 2538.4 mm wide and 507.7 mm high with flat walls as boundaries and containing 13500 particles. The thermomechanical material properties and particle size distribution are the same as those used for the previously created database of microscale results. The initial temperature of the granular material is 0 K. The bottom wall is kept at 100 K while the other boundaries are thermally insulated. The total analysis time is 5000 s and the time step used for the DEM solution is 5×10^{-4} s. The resulting wall-clock time for the full DEM computation on a standard personal desktop computer was 12.5 h.

Due to the extent of the model and the way it was created, the microstructural properties of the reference DEM model are not homogeneous across the domain, exhibiting local variations that affect the heat flux. To apply the proposed methodology, the local values of porosity and fabric are determined to serve as inputs of the previously created database in order to obtain the thermal conductivity tensors for the continuum-based model. These local values of microstructural properties are determined by dividing the domain into sub-regions where the porosity and fabric are calculated. In this case, the model was divided into a grid of 10×2 square sub-regions. A complementary analysis, not presented here for simplicity, compared the results obtained from subdivisions with different square sizes and found that the aforementioned one is optimal for faithfully capturing the local microstructural properties in this model. The maps of local porosity and fabric values are shown in Fig. 11. We remark that, in practice, when a DEM model of the material is not available, these local properties should be known a priori. This information could be obtained either by experimental analyses or by assuming a certain compaction level and type (*e.g.*, for the fabric, an isotropic compaction with $f = 0$ would often be a reasonable assumption).

Fig. 12 shows the thermal analysis solution of the reference DEM model for a temperature range of 40 K to 60 K at distinct times. It can be seen that heat flows faster near the lateral boundaries than in the central zone of the domain. This is a consequence of the lower porosity and the more accentuated fabric in the vertical direction near the lateral boundaries, which lead to higher values of the yy component of the thermal conductivity tensors in these zones, as described in the following section.

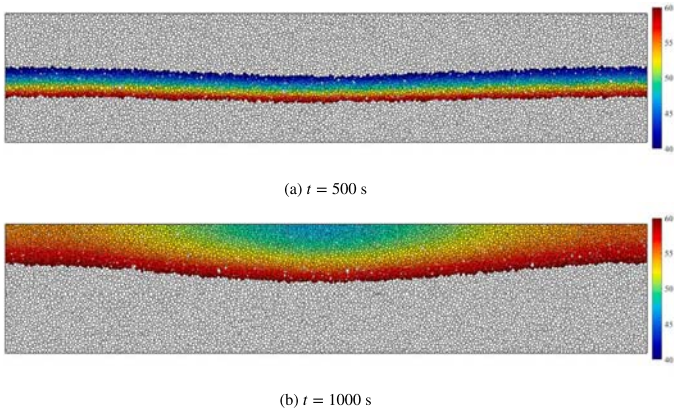

Fig. 12. Solution of reference DEM model: temperature distribution in the range of 40 K to 60 K at two time instants.

3.3.2. Continuum-based solution vs DEM solution

The FVM grid used for the continuum-based simulations of the granular medium is shown in Fig. 13. It was created by discretizing the granular domain into 1280 square cells and applying the same thermal boundary conditions and initial temperature as the reference DEM model. The density and heat capacity of the material of all cells are those provided for the solid grains. However, to obtain the effective thermal inertia, as defined in Eq. (1), the solid thermal inertia (product of density and heat capacity) is multiplied by the local porosity of each cell. The values of local porosity are those obtained directly from the reference DEM model, which are mapped in Fig. 11(a). The porosity value assigned to an FVM cell is the value of the map sub-region where the cell is located.

In order to verify the accuracy of the ML-based surrogate model, two continuum-based analyses were considered: one without and one with the incorporation of machine learning. In the analysis without machine learning, the local thermal conductivity tensors are obtained directly from the reference DEM model, by homogenization via Eq. (17) in each of the 10×2 sub-regions (*i.e.*, the sub-regions are treated as RVEs to homogenize the thermal conductivity with an online procedure). The analysis with machine learning uses the approach proposed in this work: the dimensionless thermal conductivity tensor of each sub-region is estimated from the local porosity and fabric, both mapped in Fig. 11, through the ML-based surrogate model presented in Fig. 9. The distribution of the input points of all sub-regions is illustrated in Fig. 14 across the fabric-porosity plane of the generated ANN surface for predicting the xx component of the dimensionless thermal conductivity tensor. The components of the dimensionless tensors are then scaled by the thermal conductivity of the solid grains ($k = 100$ W/mK). The resulting values of the xx and yy components of the local thermal conductivity tensors provided by the microscale surrogate model are mapped in Fig. 15. In both FVM analyses, the thermal conductivity tensor assigned to an FVM cell is the tensor of the map sub-region where the cell is located.

We highlight that we are only able to perform the analysis without machine learning because a reference DEM model was built, from which local thermal conductivity tensors can be easily computed. When such a discrete model is not available, the proposed approach allows homogenized thermal conductivities to be predicted from the locally averaged values of porosity and fabric. We also note that, in the

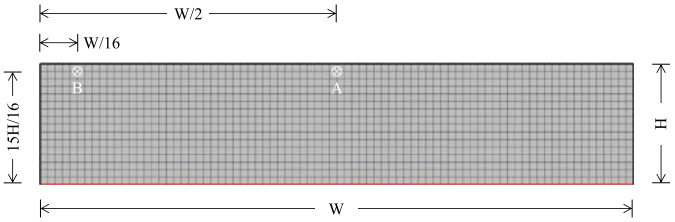

Fig. 13. FVM grid with control points A and B indicated.

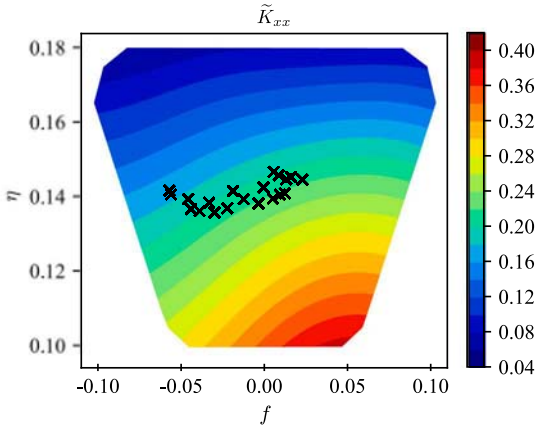

Fig. 14. Local porosities and fabrics of reference DEM model (cross symbols) depicted within the generated ANN prediction surface for the xx component of the dimensionless thermal conductivity tensor.

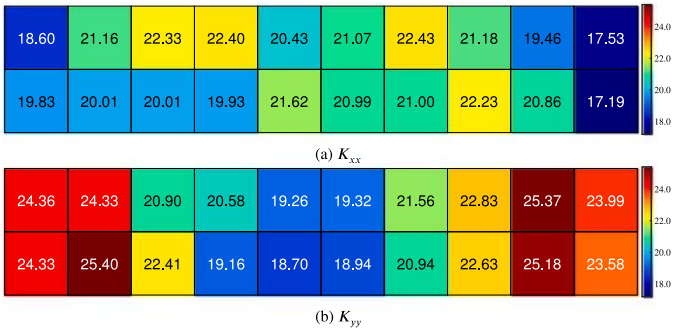

Fig. 15. Components of the local thermal conductivity tensors obtained from the microscale database by taking the local porosities and fabrics as inputs.

proposed approach, although the process of acquiring local thermal conductivity tensors for the continuous model has been performed only once, this is an online task. It means that, in the case of a transient analysis in which local properties vary over time, this process should be carried out several times along the simulation.

A time step of 1 s was employed for the FVM simulations, which ran for 5000 s. The wall-clock simulation times, using the same machine as the DEM analysis, were about 5 s. It corresponds to a speedup factor in the order of $10^4\times$ compared to the discrete method. Nevertheless, the solution of heat conduction over the granular medium was achieved with satisfactory accuracy in the continuum-based analyses, as discussed in the sequence.

The evolution of the average temperature of the discrete and continuous models is presented in Fig. 16, where the multiscale solutions refer to the continuum-based analyses without and with the incorporation of machine learning. The average temperature of the DEM model is calculated as a volume-weighted average of the particles and discarding lone elements whose temperature remains unchanged. In the FVM model,

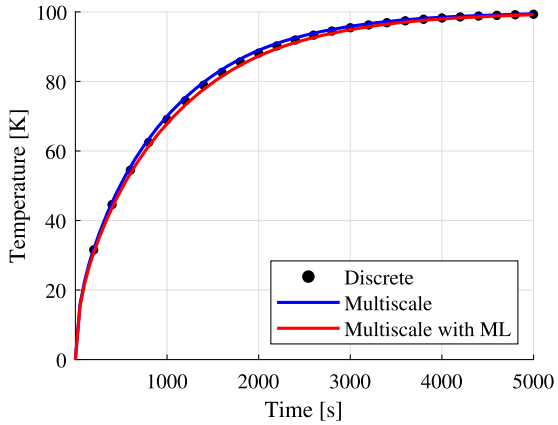

Fig. 16. Average temperature evolution from the reference discrete model (DEM) and the multiscale continuum–discrete approach (FVM) without and with machine learning (ML).

it is simply computed as the mean temperature value of all cells. The graph shows an excellent agreement between the three solutions. This indicates that, in an integral way, the heat flow is nearly identical in both discrete and continuous models. This also validates the accuracy of the ML-based surrogate model in obtaining local thermal conductivity tensors.

The temperature evolution of the discrete model and the continuous model with the proposed approach (multiscale with machine learning) is compared pointwise in the graphs of Fig. 17. The control points A and B have their positions indicated in Fig. 13. At these points, the curves also show a very good agreement, especially at point B, located near the lateral boundary, where the solutions practically overlap. Point A, located in the center of the models, is where the difference between the curves is most pronounced. In this position, the maximum error of the FVM solution against the reference DEM solution, normalized with the final equilibrium temperature (100 K), is 2.8%.

To analyze the temperature profile, Fig. 18 shows the temperature distribution in the range of 40 K to 60 K of the FVM model with the proposed approach at 500 s and 1000 s. For a qualitative comparison, the particles of the reference DEM model that are in the same range of temperature at these times, as seen in Fig. 12, are depicted with no color. It is clear that the continuum-based solution follows the same pattern as the discrete one. However, the heat flux given by the FVM solution in the central region is slightly slower than in the DEM solution. This result is clearly shown in the graphs of Fig. 19 and Fig. 20, which plot, respectively, the vertical and horizontal temperature profiles at distinct times. In Fig. 19(a), which depicts the vertical temperature profiles at the center of the model (passing through point A), the underestimation of the heat flux given by the FVM solution is noticed. This is the same discrepancy as observed in Fig. 17(a). Fig. 19(b) shows a nearly perfect agreement of the vertical temperature profiles close to the lateral boundary (passing through point B), as previously noted in Fig. 17(b). The same findings can be observed in the horizontal temperature profiles, both in the model's mid-height (Fig. 20(a)), and in the model's upper part passing through points A and B (Fig. 20(b)).

The differences encountered in the central region are the result of an underestimated thermal conductivity in the vertical direction in that zone of the FVM model. Some possible sources of error in the methodology that can explain this behavior are in the creation of the database and in the ANN model selected. Regarding the database creation, we highlight that RVEs with a sufficient number of particles can offer a good representation of a granular material, but up to a certain level of accuracy. For this reason, the results of the thermal conductivity of RVEs with the same porosity and similar fabrics present some dispersion, as seen in Fig. 6. Moreover, when preparing the database, the

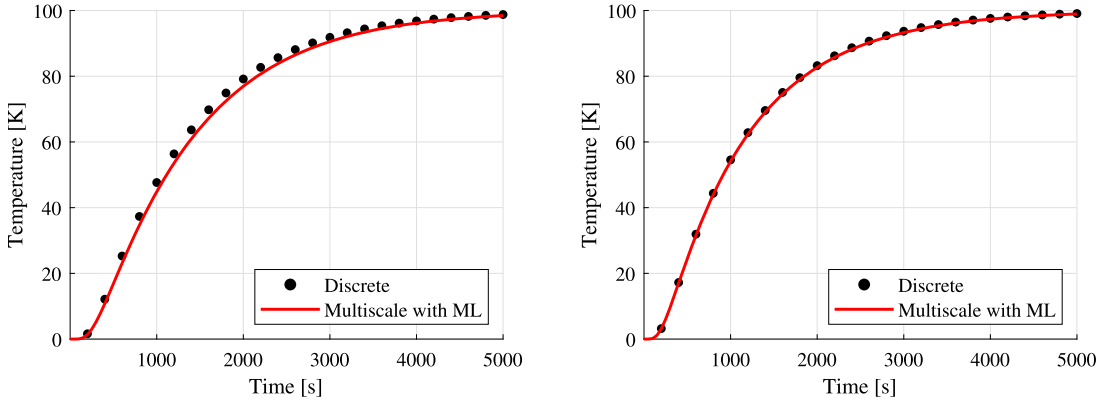

Fig. 17. Temperature evolution, at control points A and B, from the reference discrete model (DEM) and the proposed multiscale continuum–discrete approach (FVM).

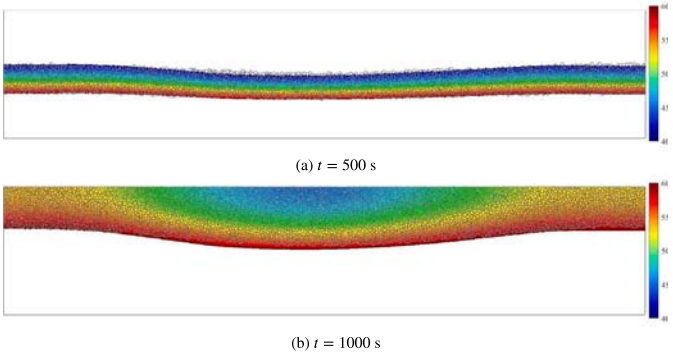

Fig. 18. Multiscale continuum–discrete solution (FVM model) compared against the reference discrete solution (DEM model): temperature distribution in the range of 40 K to 60 K at two time instants.

number and distribution of datapoints across the range of input values play an important role in estimating the outputs, as certain regions of the input space may lack sufficient data for a precise interpolation. In fact, by comparing Fig. 9a and Fig. 14, one can observe that the input points of the validation example exhibit a relatively concentrated distribution compared to the generated datapoints and part of them is situated in a sparse region of datapoints. With respect to the ANN model selected, potential sources of error were discussed in Section 3.2.2, which include the fitting error of the ANN-based surrogate model due to the influence of parameters that are not being considered as inputs of the model. The accumulation of these factors contributes to some inaccuracies in the estimation of local thermal conductivities. However, the results of the heat flux can be considered satisfactorily precise for representing a discrete solution with a continuous method.

4. Conclusions

In this work, we presented a multiscale methodology to simulate heat transfer in static granular media with a continuous numerical method by deriving effective thermal conductivity tensors via a data-driven surrogate model of microscale DEM results. The efficiency of the continuous approach relies on the creation of a database by means of the analysis of several Representative Volume Elements (RVEs) with different microstructural properties. The RVEs are generated through the compression of the particles by flat walls, and a protocol for evaluating the microstructural properties while disregarding the effects of walls was described and validated. The microscale database is used to train an artificial neural network (ANN) that serves as a surrogate model for locally relating the conductivity tensor with the porosity and fabric tensor of the material. These two local properties were demonstrated to be sufficient to estimate accurate thermal conductivity tensors, and they must be either known or assumed in advance. The results showed that the proposed methodology allows the simulation of the thermal behavior of such a complex material type with the computational performance of a continuous model and DEM-like accuracy.

The proposed multiscale approach was applied in this work with a series of simplifying considerations regarding the dimensionality of the problem. These simplifications include 2D analysis and the absence of shear effects, which enabled us, for example, to represent the fabric tensor as a single scalar parameter. As a result, the number of database inputs was minimized, and the use of an ANN could be considered an overly powerful technique for interpolating the outputs. However, the generality of the presented methodology allows it to overcome such simplifications without altering its core concepts, just by increasing the number of inputs and outputs according to the problem type. Therefore, a natural extension of this work is to consider 3D simulations with a microscale database that takes into account shear effects in the RVEs. Furthermore, a potential extension of the methodology is to incorporate the mechanical behavior of the material, which could be achieved by introducing the necessary variables, such as the stress tensor and tangent operator. If attained, the benefits of the offline microscale computations would become even more evident, as the RVEs would not need to be solved several times on the fly. All this permits us to conclude that the proposed methodology offers several possibilities for improvement in the continuum–discrete hierarchical multiscale modeling of the thermomechanical behavior of granular media.

Other developments for future work under the same numerical framework are the consideration of different heat transfer models, since the formulation presented here is particular to a thermal pipe model of heat conduction; the inclusion of the effects of interstitial air; and the assessment of the influence of different particle shapes. In addition, the database of microscale results could be generalized to any particle size distribution, possibly by generating data for several different distribution functions and including representative parameters of these functions as inputs to the ANN-based surrogate model. Finally,

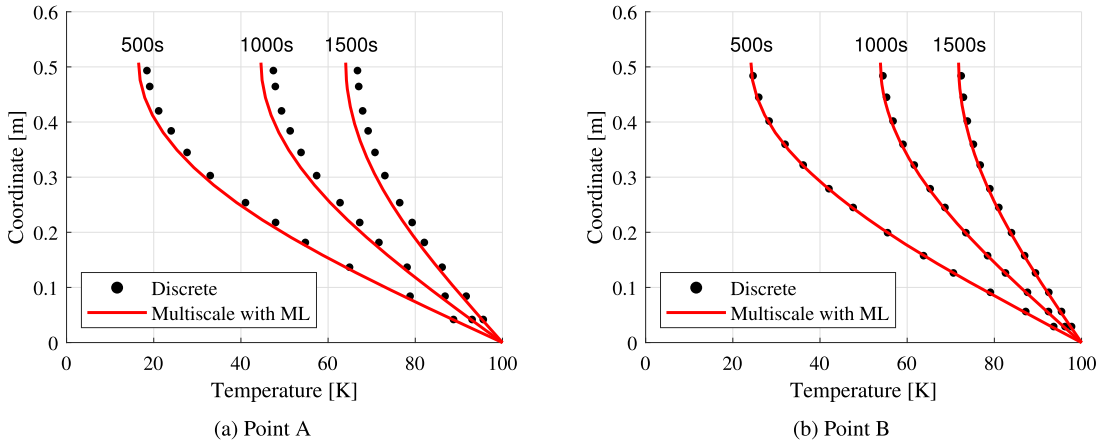

Fig. 19. Vertical temperature profiles, passing through control points A and B, from the reference discrete model (DEM) and the proposed multiscale continuum–discrete approach (FVM).

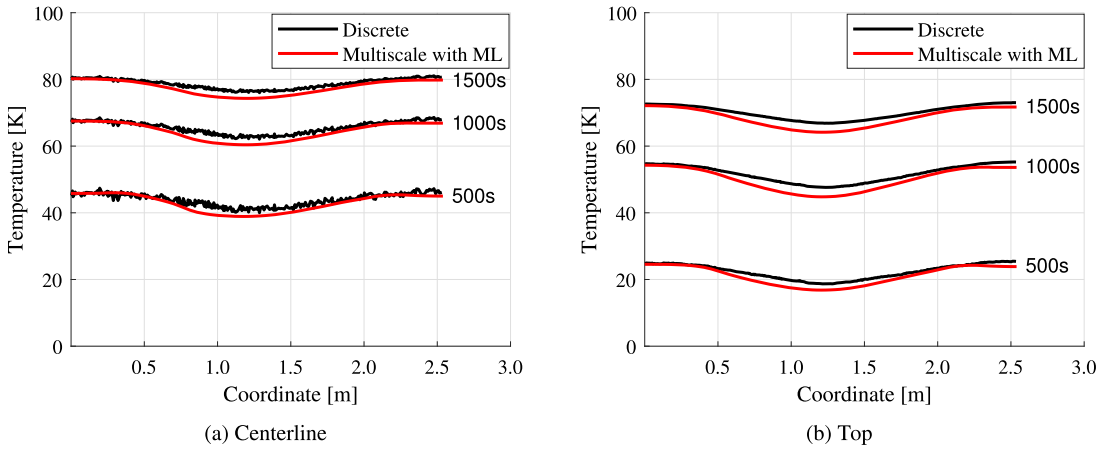

Fig. 20. Horizontal temperature profiles, passing through the mid-height (Centerline) and upper part (Top - *i.e.*, where control points A and B are located), from the reference discrete model (DEM) and the proposed multiscale continuum–discrete approach (FVM).

since the creation of databases is a time-consuming task and they can be reused in similar applications, we believe that sharing processed data for different materials, DEM models and ranges of input parameters is a good practice. The database used in this study can be found as supplementary material of the article.

CRediT authorship contribution statement

Rafael L. Rangel: Conceptualization, Formal analysis, Investigation, Methodology, Software, Validation, Writing – original draft. **Juan M. Gimenez:** Funding acquisition, Investigation, Methodology, Project administration, Software, Supervision, Writing – review & editing. **Eugenio Oñate:** Supervision, Writing – review & editing. **Alessandro Franci:** Conceptualization, Funding acquisition, Methodology, Project administration, Resources, Supervision, Writing – review & editing.

Declaration of competing interest

The authors declare that they have no known competing financial interests or personal relationships that could have appeared to influence the work reported in this paper.

Data availability

Data is provided as supplementary material.

Acknowledgments

The authors acknowledge the support from MCIN/AEI and FEDER *Una manera de hacer Europa* for funding this work via project PID2021-122676NB-I00. The authors acknowledge the Severo Ochoa Programme through the Grant CEX2018-000797-S funded by the Spanish Ministry of Economy and Competitiveness through the "Severo Ochoa Programme for Centres of Excellence in R&D". Mr. Rangel acknowledges the Marie SKŁODOWSKA-CURIE Innovative Training Network MATHEGRAM, the People Programme (Marie SKŁODOWSKA-CURIE Actions) of the European Union's Horizon 2020 Programme H2020 under REA grant agreement No. 813202, for funding his research.

Appendix A. Supplementary data

The post-processed database from RVE solutions used to train the ML model can be found online at https://doi.org/10.1016/j.compgeo.2024.106118.

References

Andrade, J., Avila, C., Hall, S., Lenoir, N., Viggiani, G., 2011. Multiscale modeling and characterization of granular matter: From grain kinematics to continuum mechanics. J. Mech. Phys. Solids 59 (2), 237–250.

Andrade, J.E., Tu, X., 2009. Multiscale framework for behavior prediction in granular media. Mech. Mater. 41 (6), 652–669.

Berzi, D., Vescovi, D., 2021. Cooling after shearing: three possible fates for dense granular materials. Granul. Matter 23 (2), 47.

Borja, R.I., Wren, J.R., 1995. Micromechanics of granular media Part I: Generation of overall constitutive equation for assemblies of circular disks. Comput. Methods Appl. Mech. Engrg. 127 (1–4), 13–36.
Bre, F., Gimenez, J.M., Fachinotti, V.D., 2018. Prediction of wind pressure coefficients on building surfaces using artificial neural networks. Energy Build. 158, 1429–1441.
Campbell, C.S., 2006. Granular material flows – An overview. Powder Technol. 162 (3), 208–229.
Cheng, H., Thornton, A.R., Luding, S., Hazel, A.L., Weinhart, T., 2023. Concurrent multi-scale modeling of granular materials: Role of coarse-graining in FEM-DEM coupling. Comput. Methods Appl. Mech. Engrg. 403, 115651.
Cundall, P.A., Strack, O.D., 1979. A discrete numerical model for granular assemblies. Geotechnique 29 (1), 47–65.
Dadvand, P., Rossi, R., Oñate, E., 2010. An object-oriented environment for developing finite element codes for multi-disciplinary applications. Arch. Comput. Methods Eng. 17, 253–297.
Gimenez, J.M., Idelsohn, S.R., Oñate, E., Löhner, R., 2021. A multiscale approach for the numerical simulation of turbulent flows with droplets. Arch. Comput. Methods Eng. 28 (6), 4185–4204.
Guo, N., Yang, Z., Yuan, W., Zhao, J., 2021. A coupled SPFEM/DEM approach for multiscale modeling of large-deformation geomechanical problems. Int. J. Numer. Anal. Methods Geomech. 45 (5), 648–667.
Guo, N., Zhao, J., 2014. A coupled FEM/DEM approach for hierarchical multiscale modelling of granular media. Internat. J. Numer. Methods Engrg. 99 (11), 789–818.
Guo, N., Zhao, J., 2016. 3D multiscale modeling of strain localization in granular media. Comput. Geotech. 80, 360–372.
Haykin, S.S., 2009. Neural Networks and Learning Machines. vol. 3, Pearson Upper Saddle River, NJ, USA.
Herrmann, H., Luding, S., 1998. Modeling granular media on the computer. Contin. Mech. Thermodyn. 10, 189–231.
Idelsohn, S., Nigro, N., Larreteguy, A., Gimenez, J., Ryzhakov, P., 2020. A pseudo-DNS method for the simulation of incompressible fluid flows with instabilities at different scales. Comput. Part. Mech. 7 (1), 19–40.
Ismail, K.A., Henrıquez, J., 2002. Numerical and experimental study of spherical capsules packed bed latent heat storage system. Appl. Therm. Eng. 22 (15), 1705–1716.
Kaneko, K., Terada, K., Kyoya, T., Kishino, Y., 2003. Global–local analysis of granular media in quasi-static equilibrium. Int. J. Solids Struct. 40 (15), 4043–4069.
Kisuka, F., Rangel, R.L., Hare, C., Vivacqua, V., Wu, C.-Y., 2023. Experimental investigation of heat generation during the mixing of granular materials using an overhead stirrer. AIChE J. e18219.
Kruth, J.-P., Wang, X., Laoui, T., Froyen, L., 2003. Lasers and materials in selective laser sintering. Assem. Autom. 23 (4), 357–371.
La Ragione, L., Magnanimo, V., 2012. Contact anisotropy and coordination number for a granular assembly: A comparison of distinct-element-method simulations and theory. Phys. Rev. E 85, 031304.
Liang, W., Zhao, J., 2019. Multiscale modeling of large deformation in geomechanics. Int. J. Numer. Anal. Methods Geomech. 43 (5), 1080–1114.
Liang, W., Zhao, J., Wu, H., Soga, K., 2023. Multiscale, multiphysics modeling of saturated granular materials in large deformation. Comput. Methods Appl. Mech. Engrg. 405, 115871.
Ma, G., Mei, J., Gao, K., Zhao, J., Zhou, W., Wang, D., 2022. Machine learning bridges microslips and slip avalanches of sheared granular gouges. Earth Planet. Sci. Lett. 579, 117366.
Meier, H.A., Steinmann, P., Kuhl, E., 2008. Towards multiscale computation of confined granular media: contact forces, stresses and tangent operators. Tech. Mech.-Eur. J. Eng. Mech. 28 (1), 32–42.
Nguyen, T.K., Combe, G., Caillerie, D., Desrues, J., 2014. FEM × DEM modelling of cohesive granular materials: numerical homogenisation and multi-scale simulations. Acta Geophys. 62, 1109–1126.
Nitka, M., Combe, G., Dascalu, C., Desrues, J., 2011. Two-scale modeling of granular materials: a DEM-FEM approach. Granul. Matter 13 (3), 277–281.
Oda, M., 1982. Fabric tensor for discontinuous geological materials. Soils Found. 22 (4), 96–108.
Qu, T., Guan, S., Feng, Y., Ma, G., Zhou, W., Zhao, J., 2023. Deep active learning for constitutive modelling of granular materials: From representative volume elements to implicit finite element modelling. Int. J. Plast. 164, 103576.
Radjai, F., Dubois, F., 2011. Discrete-Element Modeling of Granular Materials. Wiley-Iste.
Rangel, R.L., Kisuka, F., Hare, C., Vivacqua, V., Franci, A., Oñate, E., Wu, C.-Y., 2023. Experimental investigation of heat generation during granular flow in a rotating drum using infrared thermography. Powder Technol. 426, 118619.
Shahin, G., Desrues, J., Pont, S.D., Combe, G., Argilaga, A., 2016. A study of the influence of REV variability in double-scale FEM× DEM analysis. Internat. J. Numer. Methods Engrg. 107 (10), 882–900.
Versteeg, H.K., Malalasekera, W., 2007. An Introduction to Computational Fluid Dynamics: The Finite Volume Method. Pearson Education.
Vlahinić, I., Andò, E., Viggiani, G., Andrade, J.E., 2014. Towards a more accurate characterization of granular media: extracting quantitative descriptors from tomographic images. Granul. Matter 16 (1), 9–21.
Voight, B., Faust, C., 1992. Frictional heat and strength loss in some rapid landslides: error correction and affirmation of mechanism for the Vaiont landslide. Géotechnique 42 (4), 641–643.
Wang, K., Sun, W., 2018. A multiscale multi-permeability poroplasticity model linked by recursive homogenizations and deep learning. Comput. Methods Appl. Mech. Engrg. 334, 337–380.
Wang, K., Sun, W., 2019. An updated Lagrangian LBM–DEM–FEM coupling model for dual-permeability fissured porous media with embedded discontinuities. Comput. Methods Appl. Mech. Engrg. 344, 276–305.
Weller, H.G., Tabor, G., Jasak, H., Fureby, C., 1998. A tensorial approach to computational continuum mechanics using object-oriented techniques. Comput. Phys. 12 (6), 620–631.
Wiebicke, M., Andò, E., Viggiani, G., Herle, I., 2020. Measuring the evolution of contact fabric in shear bands with X-ray tomography. Acta Geotech. 15 (1), 79–93.
Yang, Z., Li, X., Yang, J., 2008. Quantifying and modelling fabric anisotropy of granular soils. Géotechnique 58 (4), 237–248.
Yue, Y., Smith, B., Chen, P.Y., Chantharayukhonthorn, M., Kamrin, K., Grinspun, E., 2018. Hybrid grains: Adaptive coupling of discrete and continuum simulations of granular media. ACM Trans. Graph. 37 (6).
Zhang, H., Zhou, Q., Zheng, Y., 2011. A multi-scale method for thermal conduction simulation in granular materials. Comput. Mater. Sci. 50 (10), 2750–2758.
Zhao, S., Zhao, J., Lai, Y., 2020. Multiscale modeling of thermo-mechanical responses of granular materials: A hierarchical continuum–discrete coupling approach. Comput. Methods Appl. Mech. Engrg. 367, 113100.
Zhao, S., Zhao, J., Liang, W., Niu, F., 2022. Multiscale modeling of coupled thermo-mechanical behavior of granular media in large deformation and flow. Comput. Geotech. 149, 104855.
Zhou, Z., Yu, A., Zulli, P., 2009. Particle scale study of heat transfer in packed and bubbling fluidized beds. AIChE J. 55 (4), 868–884.
Zienkiewicz, O.C., Taylor, R.L., Zhu, J.Z., 2005. The Finite Element Method: Its Basis and Fundamentals. Elsevier.